ACS Photonics

pubs.acs.org/journal/apchd5

Article

Reconfigurable Frequency-Selective Resonance Splitting in Chalcogenide Microring Resonators

Bin Shen, Hongtao Lin, Saeed Sharif Azadeh, Jovana Nojic, Myungkoo Kang, Florian Merget, Kathleen A. Richardson, Juejun Hu, and Jeremy Witzens*

Cite This: *ACS Photonics* 2020, 7, 499–511

Read Online

ACCESS | Metrics & More | Article Recommendations | Supporting Information

ABSTRACT: This paper reports a method to enable, for the first time, reconfigurable control of resonance splitting of one or multiple arbitrarily selected azimuthal orders in a microring resonator. This is accomplished by inscribing Bragg gratings in photosensitive $Ge_{23}Sb_7S_{70}$ chalcogenide microring resonators via a novel cavity-enhanced photoinscription process, in which injection of light at the targeted C-band resonance frequency induces a spatially varying refractive index change. The so-formed Bragg grating precisely matches the selected resonance order without introducing optical losses. Long-term room temperature stability of the photoinscribed Bragg gratings has been verified in darkness and during operation with reduced optical power levels. The Bragg gratings can be reconfigured by first erasure with flood illumination of visible light at 561 nm and subsequent reinscription. We also report controlled splitting of multiple resonances by inscribing superimposed Bragg gratings.

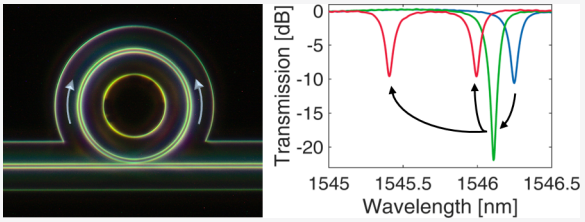

KEYWORDS: *chalcogenide photonics, reconfigurable photonics, resonance splitting*

Mode splitting in microring and fiber ring resonators has been used for optical label-free biosensing,[1] nanoparticle detection,[2] and strain sensing.[3] Each resonator mode is naturally 2-fold degenerate, as the clockwise (CW) and counterclockwise (CCW) propagating modes share a common resonance frequency. In case the CW and CCW modes are coupled with each other by intracavity back-reflections, the degeneracy is lifted, with mode frequencies splitting as a result.[4] In some of the aforementioned sensing applications, backscattering is induced by the presence of nanoparticles, either as a consequence of a detected molecule being present or as the direct target of the sensor.[1,2] In others, insertion of a fiber Bragg grating (FBG) in a ring resonator allows for a highly phase-sensitive readout of its properties.[3] Mode splitting and the resulting change of the device's transfer function has also been used to engineer the transfer function of optical filters.[5] In addition to their broad impacts on sensing and filtering, further applications of resonance-splitting in waveguide coupled ring resonators include frequency selective back-reflectors in external cavity lasers.[6] Since, in the presence of resonance-splitting, each hybrid mode consists in a superposition of the two counter-propagating waves, a back-reflection is also induced in the coupled bus waveguide at the split resonance frequencies.

Mode splitting in ring resonators has been widely studied.[7−9] However, naturally occurring backscattering, such as that induced by waveguide sidewall roughness or scattering from directional couplers, is a random process highly dependent on the fabrication protocols or, in the latter case, a device nonideality. Controlled mode splitting has been experimentally demonstrated by placing Rayleigh scatterers in whispering-gallery-mode microresonators,[10] inserting Bragg gratings in fiber ring resonators,[3] introducing feedback from a coupled waveguide,[11] or by evanescently coupling separate sections of the ring with each other.[5] However, in these examples, the mode splitting occurs simultaneously at all or a large number of resonances, thus limiting its application to filters or frequency selective back-reflectors. Splitting at a single resonance has been demonstrated in silicon microring resonators by embedding gratings satisfying the Bragg condition for a single azimuthal mode into the microring.[12] In this approach, however, the performance of the designed devices is limited by the resolution and accuracy of the fabrication technology. Controlled splitting of multiple selected modes requires complex superimposed Bragg gratings and has, to the best of our knowledge, not yet been realized by this method. Moreover, once fabricated, the engraved Bragg gratings are not reconfigurable.

Nonvolatile reconfigurable optics, on the other hand, have received considerable attention in recent years.[13−16] A large span of applications such as the passive biasing of Mach−Zehnder modulators[17] and low power optical switches,[18] as

Received: November 5, 2019
Published: January 8, 2020

https://dx.doi.org/10.1021/acsphotonics.9b01593
ACS Photonics 2020, 7, 499−511

Table 1. Characteristics and Measured Performance Metrics of Measured Devices[a]

device	cladding	W (nm)	H (nm)	γ	n_{eff}	radius (μm)	gap (nm)	FSR (nm)	ER (dB)	loaded Q	PE (dB)	GC back-reflection (%)
A	SiO_2	900	500	0.83	1.80	15	200	10.3	10.1	14000	14.1	2.9
B	SiO_2	950	500	0.84	1.81	15	200	10.3	9.6	19000	16.0	4.0
C	air	900	500	0.85	1.77	50	150	3.0	22.4	26000	12.0	2.9
D	SiO_2	900	500	0.83	1.80	75	250	2.1	10.6	67000	14.4	2.3

[a]W, waveguide width; H, waveguide height; γ, modeled fraction of the power confined inside the waveguide core; n_{eff}, modeled effective index; gap, spacing between ring and bus waveguide; FSR, measured free spectral range; ER, measured extinction ratio at resonance; loaded Q, measured loaded Q-factor; PE, enhancement of power circulating inside the ring relative to the bus waveguide, modeled taking into account measured FSR, extinction, and loaded Q-factor; GC back-reflection extracted from measured ripples in device transfer functions.

well as more future-looking applications, such as optical nonvolatile multilevel memories[19] and adaptive neural networks,[20] illustrate the relevance of photonic integrated circuit reconfigurability. Approaches for the latter in particular have included remanently changing the optical properties of ring resonators with phase change materials. Ring resonators have also been identified as an essential building block for some reservoir computing architectures[21] that may benefit from reconfigurability.

In this paper, we demonstrate an approach to selectively split one or multiple resonances by inscribing Bragg gratings to chalcogenide microring resonators exploiting cavity-enhanced photosensitivity of $Ge_{23}Sb_7S_{70}$ (GeSbS) chalcogenide glass at 1550 nm. Gratings are inscribed after the fabrication of the GeSbS ring resonators by injecting light into the bus waveguide to which the ring is coupled at the targeted C-band resonance frequency. Resonant enhancements in the range of 12 to 16 dB result in high power levels inside the rings (>150 mW), enabling the writing process even at moderate bus waveguide power (<10 mW). This approach eliminates the need for precise lithographic control of the grating shape and enables writing in a matter of minutes (<3 min). The long-term room temperature stability of the Bragg gratings has been verified in darkness and during operation with reduced optical power levels (10 mW inside the ring). The Bragg gratings can be controllably erased by flood illumination with shorter wavelength light (here, λ = 561 nm). Mode splitting can be subsequently reapplied, making it reconfigurable. Furthermore, splitting of multiple resonances by inscribing superimposed Bragg gratings is shown.

Chalcogenide glasses are an important class of semiconducting compounds, which contain one or more of the chalcogen elements including S, Se and Te and are covalently formed with network formers such as Ge, Sb or As.[22] Their photosensitivity is a well-known property, which has been exploited to write optical waveguides,[23] to adjust the optical properties of photonic crystal cavities,[24] to trim the resonance wavelength of ring resonators[25] and microdisks,[26] or to tune directional couplers.[27] Additionally, photosensitivity of chalcogenide glasses has been applied to write Bragg gratings in chalcogenide waveguides by external illumination with visible light,[28,29] as well as by injecting infrared light at the wavelength of 1550 nm.[30] In the visible wavelength range with photon energies close to the bandgap of the chalcogenide glasses, photosensitivity is known to be due to structural rearrangements triggered by absorption of the light.[31] Structural rearrangements such as bending, breaking, or reforming have been observed in a wide range of chalcogenide glass systems, including Ge−Sb−S/Se, As_2S_3, and As−Se.[32−34] The photosensitivity can generate electronic defects, thereby often leading to postfabrication structural instability. Particularly, this is an issue for As_2Se_3. Ge-doped As−Se has been proposed as a compositionally engineered alternative that possesses both photosensitivity and structural stability. As a result of the photoinduced structural rearrangement, both positive and negative refractive index changes have been observed under external illumination with visible light.[35] At 1550 nm, photosensitivity of the chalcogenide As_2S_3 glasses has been attributed to the absorption by subgap defects.[26] However, since defect density and energy are highly process- and material-dependent, nonlinear multiphoton absorption cannot be excluded to also play a role in other works.[36−38]

In this paper, we first discuss the materials, device fabrication, and principle of Bragg grating inscription leading to resonance splitting. Following this, we present the experimental demonstration of a single resonance splitting. Next, we study the short- and long-term stability of the splitting in darkness and under reduced power device operation in the C-band. A systematic study of the refractive index shifting rates reveals a threshold-like behavior and that the sign of the photosensitivity depends on optical power levels. We then investigate erasure of the splitting by overwriting of the Bragg gratings with flood illumination by visible light. Subsequent rewriting of Bragg gratings is reported in Supporting Information, SIV. Finally, we study the inscription of superimposed Bragg gratings and the splitting of multiple selected resonances.

MATERIALS AND METHODS

Four devices, henceforth referred to as devices A, B, C, and D, are used to conduct the experiments reported in this paper. Each consists of a GeSbS ring resonator coupled to a 244 μm long bus waveguide. These are connected to a pair of fully etched GeSbS focusing grating couplers (GCs)[39] to facilitate optical interrogation with standard single-mode fibers. Table 1 summarizes the device characteristics. In all four, GeSbS waveguides are fabricated out of a 500 nm thick film deposited on top of an oxidized silicon wafer with a 3 μm thick SiO_2 layer by single-source thermal evaporation.[40] Waveguides and GCs are defined by electron beam lithography (EBL) and fully etched by reactive ion etching with CHF_3/CF_4 (3:1).[41] Devices were subsequently measured without prior annealing of the GeSbS.

Except device C, all other devices were covered by a 200 nm SiO_2 top cladding layer. Resulting changes in effective and group indices are easily taken into account in the device models, so that this does not limit comparison between experiments. The fraction of the optical power contained in the core (γ) only changes marginally and remains very high in both cases (Table 1). The fraction in SiO_2 increases from 9% to 15% as the top SiO_2 layer is being added, but remains low, so that the optical properties of the waveguide are not

https://dx.doi.org/10.1021/acsphotonics.9b01593
ACS Photonics 2020, 7, 499−511

significantly modified. The initial purpose of the top cladding layer had been to improve the robustness against high optical power levels, but for the range of experiments reported here, this did not appear to play a role. Moreover, no other differences have been observed between these two types of waveguides. Two factors are of particular importance to model the resonance splitting process: (i) the power enhancement factor inside the resonator, which depends on the ring to bus waveguide coupling coefficient, the loaded quality (Q)-factor, and the free spectral range (FSR), as well as (ii) back-reflection at the output GC, which acts as a seed for the standing wave leading to the remanent Bragg grating formation inside the ring. While all the GCs followed the same design principle, period and pitch were slightly varied in between devices, which resulted in varying reflection coefficients that can be independently extracted from the ripples in the spectrally resolved optical transfer functions.[39]

Figure 1a illustrates the process leading to the inscription of Bragg gratings in the GeSbS ring resonators under strong

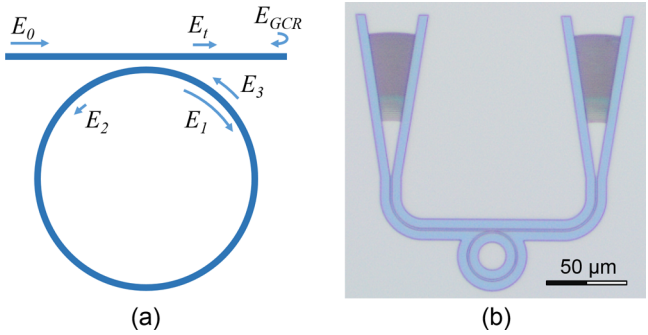

Figure 1. (a) Schematic diagram of the process used to write Bragg gratings in the rings. (b) Optical microscope image of a GeSbS ring resonator with bus waveguide and GCs.

optical excitation at a resonance wavelength (λ_0). This process is seeded by a small reflection from the output GC, leading to a portion of the field transmitted past the ring resonator (E_t) to be reflected back (E_{GCR}). This, in turn, leads to a weak counter-propagating CCW wave to enter the resonator (E_2) and to interfere with the forward propagating CW wave (E_1). Together, they form a standing wave that is converted into a Bragg grating via the material photosensitivity. The period Λ of the standing wave pattern can be simply calculated as

$$\Lambda = \frac{\lambda_0}{2n_{\text{eff}}} \tag{1}$$

with n_{eff} being the waveguide's effective index. It has exactly the right value to couple the CW and CCW waves to each other at λ_0.

The CW wave (E_1) is then directly back-reflected inside the ring (E_3). Since the grating was seeded by the initial (parasitic) CCW wave E_2, the back-reflection E_3 is generated coherently and reinforces E_2, accelerating and self-reinforcing the grating formation under appropriate conditions (see below).

The Bragg grating field reflectivity r_B can be derived as[42,43]

$$r_B = \frac{-K \sinh(\Theta L)}{\Theta \cosh(\Theta L) - j\Delta\beta \sinh(\Theta L)} \tag{2}$$

with L being the length of the Bragg grating, here the circumference of the ring. Θ and $\Delta\beta$ can be expressed as $\Theta = \sqrt{K^2 - \Delta\beta^2}$ and $\Delta\beta = 2\pi n_g(\lambda_B - \lambda)/(\lambda_B\lambda)$, with K being the coupling rate between the forward and backward propagating waves, $\lambda_B = \lambda_0$ is the center wavelength of the Bragg grating (which is also the resonance wavelength of the ring), and λ is the wavelength of the light. K is given by $\pi\Gamma\Delta n_B/(2\lambda)$ for a sinusoidal index modulation,[43] wherein Δn_B is the peak-to-peak refractive index modulation of the Bragg gratings and $\Gamma = \gamma(n_g/n_{\text{GeSbS}})$ is the modal confinement factor. γ is simply defined as the fraction of the power confined inside the waveguide core, n_g is the group index of the waveguide, and n_{GeSbS} is the refractive index of the core material. The term n_g/n_{GeSbS} is a corrective factor accounting for slow light effects in high index contrast waveguides.[44,45] At $\lambda_B = \lambda_0$, this reduces to

$$r_B = -\tanh(KL) = -\tanh\left(\frac{\pi\Gamma\Delta n_B}{2\lambda}L\right) \tag{3}$$

It should be noted that the average refractive index of the GeSbS glass also changes during the Bragg grating writing process, which results in a shift of the resonance wavelength. Therefore, the wavelength of the light needs to be actively tuned by a minimum transmission tracker to keep it on resonance. Since the change in the refractive index is then compensated by the change of the resonance wavelength, the period of the written Bragg grating stays constant. Once splitting occurs, the wavelength of light is set to track the resonance with the higher frequency, which corresponds to a standing wave with field maxima at the index of refraction minima. Since at high power levels the material exhibits a negative photosensitivity,[33,46] this process reinforces the pre-existing grating pattern. Continuous high-power exposure at the wavelength of the other split resonance is expected, on the other hand, to result in a reduction of the splitting strength. The writing process duration is henceforth referred to as the exposure time.

The field transmission $t = E_t/E_0$ is modeled as[47]

$$t = 1 - \frac{1}{2Q_c}\left(\frac{(1+f)^2}{j\left(\delta + \frac{1}{2Q_r}\right) + \frac{1}{2Q_i} + \frac{1}{2Q_c}} + \frac{(1-f)^2}{j\left(\delta - \frac{1}{2Q_r}\right) + \frac{1}{2Q_i} + \frac{1}{2Q_c}}\right) \tag{4}$$

where Q_i and Q_c are the intrinsic and coupling Q-factors defined as $Q_i = \omega_0\tau_i/2$ and $Q_c = \omega_0\tau_c/2$. τ_i and τ_c are the photon life times limited by the intrinsic loss and waveguide coupling, respectively. $\delta = (\omega - \omega_0)/\omega_0$ is the normalized frequency detuning and f describes the asymmetry of the extinction induced by the two hybridized modes. It is a consequence of the forward propagating wave inside the bus waveguide coupling to both the CW and CCW resonator modes,[6] which happens here indirectly via the back-reflection at the output grating coupler. $Q_r = \omega_0/(2\mu)$ is the mutual-coupling Q-factor,[8,48] with μ being the mutual-coupling coefficient between the CW and CCW modes. The relation between the field amplitude reflectivity and the time-domain mutual-coupling coefficient is[9,48]

https://dx.doi.org/10.1021/acsphotonics.9b01593
ACS Photonics 2020, 7, 499−511

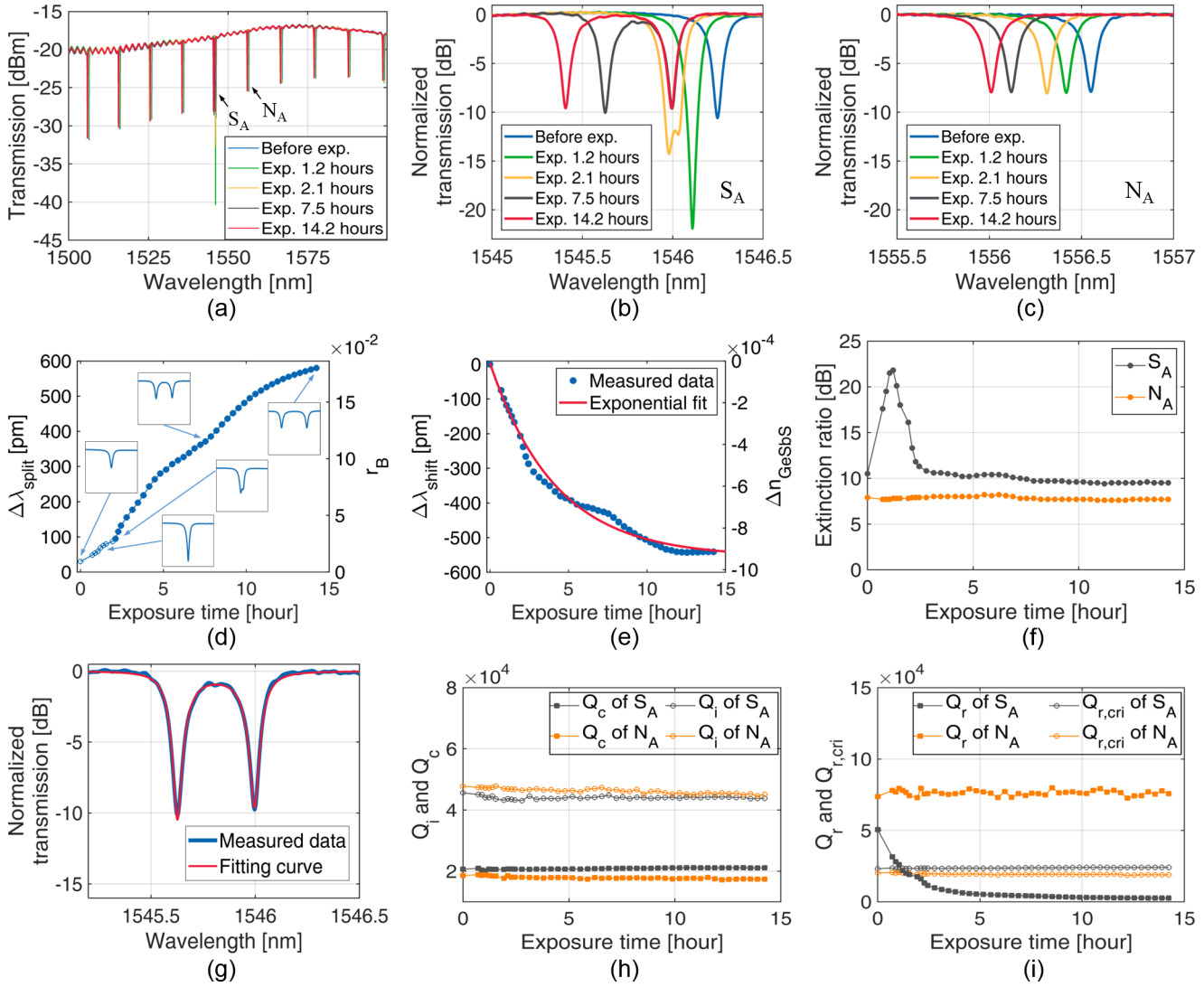

Figure 2. Dynamics of the splitting process. (a) Transmission spectra of device A before and during exposure. Normalized transmission spectra of (b) the split resonance S_A and (c) the adjacent resonance N_A before and during exposure. (d) Splitting width $\Delta\lambda_{split}$ of resonance S_A and corresponding Bragg grating field reflectivity r_B vs exposure time. The solid dots are measured data. The hollow dots before 2.1 h are obtained through resonance fitting, since splitting is not directly visible during this time. Insets: Normalized transmission spectra of S_A in a wavelength range of 1.2 nm around the resonance and normalized power range between −25 and 5 dB. (e) Wavelength shift $\Delta\lambda_{shift}$ of N_A and the corresponding GeSbS refractive index change as a function of exposure time. (f) Extinction ratio of S_A and N_A before and during exposure. (g) Measured spectrum (blue) and fit (red) of S_A after 7.5 h exposure. (h) Extracted intrinsic (Q_i) and coupling (Q_c) Q-factors of S_A and N_A before and during exposure. (i) Mutual-coupling (Q_r) and critical mutual-coupling ($Q_{r,cri}$) Q-factors before and during exposure. Power levels were chosen to result in a slow and easily resolved splitting process. Much faster reconfiguration on the order of minutes is reported in the following sections.

$$r_B = \mu\frac{n_g L}{c_0} = \frac{\pi\Delta\lambda_{split}}{FSR} \quad (5)$$

with c_0 being the speed of light in vacuum and $\Delta\lambda_{split}$ is the splitting width. Thus, r_B and Δn_B are directly accessible from measured transmission spectra.

Instead of relying on spurious GC back-reflection, the grating formation could also have been seeded by injecting counter-propagating waves into the two ends of the bus waveguide. However, the method used here has the benefit of providing a stable phase relation between counter-propagating waves irrespectively of the phase stability of external fiber-based optics.

SINGLE RESONANCE SPLITTING

Single resonance splitting is demonstrated with device A. Before the splitting process, we measure the transmission spectrum of the device with a low input power (blue curves in Figure 2a−c). All transmission spectra reported in this paper were measured with 0 dBm inside the fiber, resulting in the power inside the bus waveguide to be in the range of −10.8 to −8.2 dBm, depending on the device. Moreover, for all measurements the temperature of the vacuum chuck holding the samples was stabilized at 25 °C in order to minimize the impact of temperature drift on the recorded resonance positions.[49] From the transmission spectrum shown in Figure 2a, the FSR of the ring resonator is measured to be 10.3 nm. The loaded Q-factor is extracted as 14000 from the transfer function of the device. These result in a power enhancement factor inside the ring of 14.1 dB. The resonance at the

https://dx.doi.org/10.1021/acsphotonics.9b01593
ACS Photonics 2020, 7, 499−511

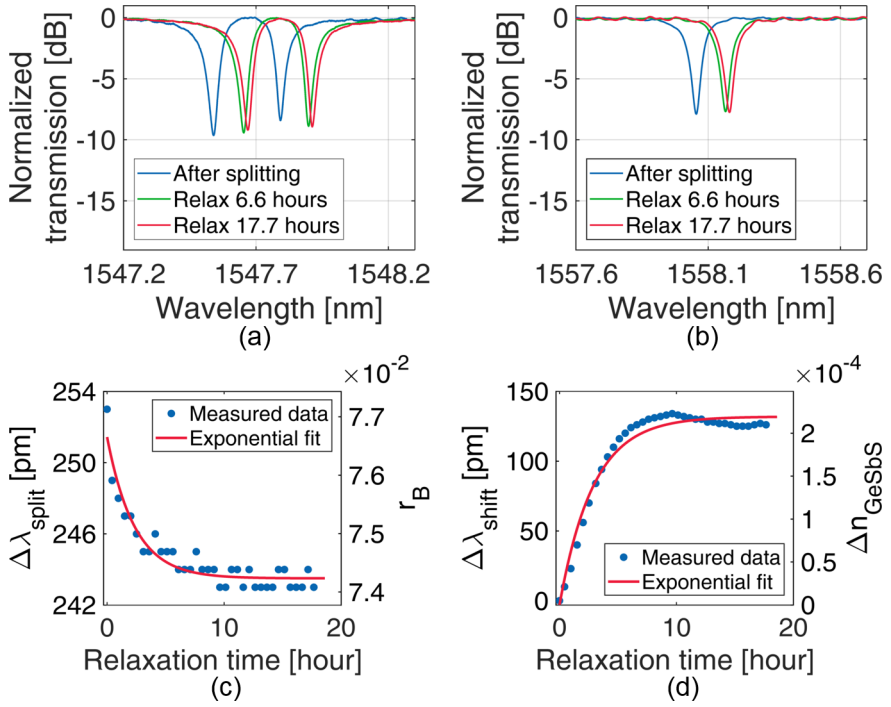

Figure 3. Short-term stability of the induced splitting. Normalized transmission spectra of (a) the split resonance S_B and (b) the adjacent resonance N_B (device B) during short-term relaxation in darkness. (c) Splitting width of S_B and corresponding Bragg grating field reflectivity against relaxation time. (d) Resonance shift of N_B and corresponding GeSbS refractive index change.

wavelength of 1546.3 nm (S_A) is selected for splitting. The adjacent resonance at 1556.6 nm (N_A) is monitored to track the overall resonance wavelength shift as well as to monitor the influence of the splitting process on neighboring resonances. The transmission spectrum of the grating coupler loop contains a 0.5 dB Fabry−Perot ripple due to the back-reflection between the input and output GCs, as evidenced by the ripple FSR of 2.0 nm. It allows us to calculate that 2.9% of the light is back-reflected by each GC. During exposure, we set the power inside the bus waveguide to 7.8 dBm, corresponding to 28 MW/cm^2 inside the core of the ring.

Figure 2b shows the transmission spectra of the resonance S_A, before and during the exposure process. During exposure, S_A blue shifts and mode-splitting starts to appear (Figure 2d). In addition, the extinction on resonance first increases and reaches critical coupling after 1.2 h of continuous exposure, after which it returns to comparable levels as observed at the beginning of the process. Fitting of the split resonances with eq 4 shows that the intrinsic and coupling Q-factors Q_i and Q_c remain unaffected by the exposure (Figure 2h). Rather, the critical coupling point is modified due to Mie-splitting.[47] At fixed Q_i and Q_c, critical coupling is reached for an initially overcoupled ring ($Q_c < Q_i$) for a mutual-coupling Q_r given by

$$\frac{1}{Q_{r,cri}^2} = \frac{1}{Q_c^2} - \frac{1}{Q_i^2} \tag{6}$$

This also allows us to unambiguously determine that the ring was initially overcoupled and to classify Q_i and Q_c in Figure 2h. For exposure times below 2.1 h, no visible splitting is observed in the spectrum of S_A. The splitting width (wavelength difference between the nondegenerate resonances) in this period is calculated by fitting the resonance (hollow dots in Figure 2d). After exposure for 2.1 h, a visible splitting is observed in the spectrum of S_A. The splitting width can then be directly read from the spectra as the measured wavelength difference between transmission minima (solid dots in Figure 2d). Once splitting becomes visible, a strong standing wave builds up inside the resonator, resulting in the splitting to grow at an accelerated rate, confirming the self-reinforcing nature of the writing process. After 14.2 h of exposure, the splitting width reaches 586 pm (Figure 2d). We extract the Bragg grating reflectivity r_B from the splitting width (Figure 2d). It reaches 0.18 after 14.2 h exposure. Based on eq 3, we estimate the refractive index modulation Δn_B to be 2.0×10^{-3}.

Figure 2c shows the transmission spectra of the adjacent resonance N_A before and during exposure. As all other resonances excluding S_A, it does not split. Furthermore, the extinction ratio and Q-factor of N_A do not change during exposure (Figure 2f,h). However, its resonance wavelength does blue shift ($\Delta\lambda_{shift}$), as observed for all other resonances. The average refractive change of the GeSbS glass is inferred from the blue shift of the unsplit resonances via[26,45]

$$\Delta n_{GeSbS} = \frac{\Delta\lambda_{shift} n_g}{\lambda\Gamma} = \frac{\Delta\lambda_{shift} n_{GeSbS}}{\lambda\gamma} \tag{7}$$

Figure 2e shows the resonance shift of N_A and the extracted average refractive index shift against exposure time. The shifts slow down as the exposure time increases and eventually saturate at −541 pm and -9.1×10^{-4}, respectively. The $1/e$ time constant of the exponential fits is 4.0 h. Uncoincidentally, the peak-to-peak index modulation Δn_B is approximately twice Δn_{GeSbS}, indicating the inscribed grating to have a high contrast ratio.

By fitting the resonance N_A, we extract the Q-factors Q_i, Q_c, and Q_r during exposure (Figure 2h,i). They remain constant, which shows that the exposure process only selectively changes the Q_r of S_A and does not influence other resonances of the ring resonator other than an overall wavelength shift.

https://dx.doi.org/10.1021/acsphotonics.9b01593
ACS Photonics 2020, 7, 499−511

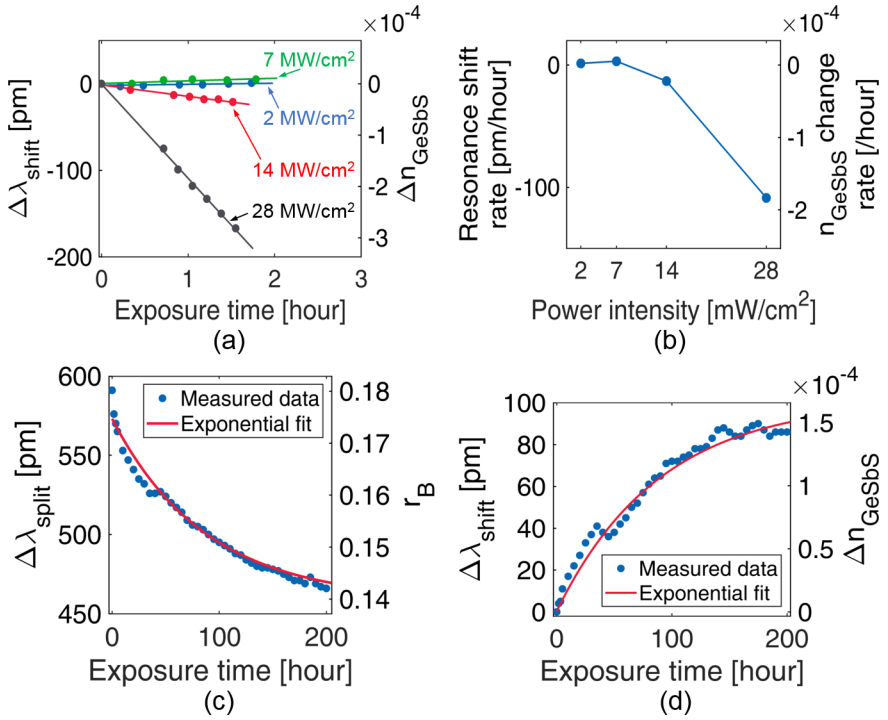

Figure 4. (a) Resonance shift of S_A vs exposure time, with varying power intensities injected at resonance wavelength S_A. (b) Rate of resonance shift vs power intensity inside the ring. (c) Splitting width of S_A and corresponding Bragg grating field reflectivity against exposure time at reduced power density (2 MW/cm^2 inside the ring). (d) Resonance shift of N_A and corresponding GeSbS refractive index change against exposure time at reduced power density.

We have also monitored the back-reflection induced by the selective resonance splitting (Supporting Information, SIII).

RESONANCE SPLITTING STABILITY IN DARKNESS AND UNDER OPERATION

Stability of the induced splitting is investigated in darkness with devices B and C and under operation with device A. Short-term stability of the splitting in darkness is first studied with device B. An FSR of 10.3 nm and a loaded Q-factor of about 19000 result in an optical power enhancement factor of 16.0 dB. 4.0% GC back-reflection is extracted from the 0.7 dB Fabry−Perot ripples.

The resonance at the wavelength of 1549.3 nm (S_B) is selected for splitting. The adjacent resonance at 1559.6 nm (N_B) is monitored to track the resonance wavelength shift. Device B is exposed 10 min to light at the resonance wavelength S_B with a power intensity of 120 MW/cm^2 inside the core of the resonator, resulting in a splitting width of 253 pm. The chip is then kept in darkness for 17.7 h, while remaining temperature stabilized at 25 °C, during which the device spectrum is periodically remeasured. Figure 3a,b show the normalized transmission spectra of S_B and N_B at various times after splitting. Both the splitting of resonance S_B, as well as the overall resonance shift monitored with N_B, undergo a small degree of relaxation. The splitting width decreases by 10 pm and stabilizes at 243 nm after ∼7 h, indicating that about 96% of the induced splitting is maintained after short-term relaxation. The $1/e$ time constant of the exponential fit is 2.3 h. The small ripples in Figure 3c are due to the resolution limit of the measurement equipment. The extracted Bragg grating reflectivity decreases from 0.077 to 0.074, the corresponding index modulation from 8.6×10^{-4} to 8.3×10^{-4}.

During the splitting of S_B, the resonance has a blue shift of 1.59 nm, which corresponds to an average GeSbS refractive index change of -2.6×10^{-3}. This points to the average refractive index shifting much more relative to the grating strength in this accelerated, increased power splitting process. During the relaxation in darkness, the resonances red shift. Figure 3d shows the recorded red shift of N_B (blue dots) as well as its exponential fit (red curve). The red shift also saturates after ∼7 h, with a comparable fitted $1/e$ time constant of 2.6 h. It stabilizes at about 0.13 nm from its value right after splitting, corresponding to a similar degree of relaxation (92% of the resonance shift remains).

Since device B was subsequently used for a splitting erasure test reported later, we used device C to study the long-term stability of the resonance splitting over a range of 9 months. An FSR of 3.0 nm and a loaded Q-factor of about 26000 result in an optical power enhancement factor of 12.0 dB. We extract a 2.9% GC back-reflection from the 0.5 dB Fabry−Perot ripples. The power inside the bus waveguide was increased to 15.1 dBm at the selected resonance wavelength to produce the splitting. After 10 min exposure with a power intensity of 97 MW/cm^2 inside the resonator core, 72 pm resonance splitting was induced. Next, the chip was removed from the temperature-controlled vacuum chuck and kept in a dark box at room temperature. The transmission spectrum of the device was remeasured after 4 and 9 months of storage. The widths of the splitting after 4 and 9 months are both 55 pm, which indicates the splitting width to be already fully stabilized at month 4, consistent with previously reported relaxation studies.[46] About 76% of the initial resonance splitting width remains after long-term relaxation (see Supporting Information, SVI). While device C is the only one with an air cladding used in the studies reported in the main part of this paper, it

https://dx.doi.org/10.1021/acsphotonics.9b01593
ACS Photonics 2020, 7, 499−511

was picked for the long-term reliability study purely as a coincidence. A device sealed from atmosphere with an SiO_2 cladding might be even more reliable.

In order to better understand the threshold of the splitting process, we have studied the relation between the photosensitivity of the GeSbS glass film and the power intensity of the light injected in the ring resonator, using device A prior to resonance splitting.

Figure 4a shows the resonance shifts of S_A as well as the extracted refractive index change against exposure time, injecting light with different power intensities at the resonant wavelength. The last data set with power density 28 MW/cm^2 corresponds to the beginning of the splitting process reported earlier. The resonance S_A slightly red shifts at low power intensities of 2 and 7 MW/cm^2, while it significantly blue shifts at high power intensities of 14 and 28 MW/cm^2. Such trends have been previously observed in other chalcogenide materials,[35] in which it was attributed to a combination of photoexpansion[33,50] at low and photobleaching at high power levels.

We extract the rates of resonance shift at different power intensities from linear fits of the measurement data (Figure 4b). As we increase the intensity inside the ring from 2 to 7 MW/cm^2, the rate of the resonance shift increases from 1.3 to 3.0 pm/h, corresponding to the GeSbS refractive index change increasing from 2.1×10^{-6} to 5.1×10^{-6} RIU/h. When we further increase the intensity to 14 MW/cm^2, the rate of resonance shift turns negative to −13.2 pm/h (-2.2×10^{-5} RIU/h). Further increasing the intensity to 28 MW/cm^2 enhances the negative rate of resonance shift to −108.7 pm/h (-1.8×10^{-4} RIU/h). Since at high intensity levels doubling the optical intensity results in an ∼8× increase in the refractive index's rate of change, negative refractive index changes could be related here to three-photon absorption, consistent with the photon energy being close to one-third of the ∼2.5 eV bandgap.

Since light induces a photoresponse in the ring, even at low power densities, the question is being raised whether splitting of resonances remains stable during long-term, low-power operation of the device. Since at reduced power levels the photosensitivity has an opposite sign, the standing wave building up inside the ring may reduce the grating strength if here too light is being injected in the higher frequency split resonance. Therefore, we measured the stability of the splitting of resonance S_A of device A while injecting moderate power levels at a wavelength tracking the higher frequency split resonance. After splitting S_A with an optical intensity of 28 MW/cm^2 inside the ring, as reported earlier in this paper, we reduced the optical intensity to 2 MW/cm^2, corresponding to a power of 10 mW inside the ring. As before, we monitor the splitting of S_A and the resonance wavelength of N_A.

Figure 4c shows the splitting width of S_A against reduced power exposure time. As expected, the splitting width reduces during reduced power exposure, rather than continuing to grow, from 586 to 466 pm after continuous reduced power exposure over 200 h. The corresponding Bragg grating reflectivity reduces from 0.181 to 0.143. Based on an exponential fit, we expect the splitting width to stabilize at 457 pm with a $1/e$ time constant of 87.5 h, so that 78% of the initial split remains.

Figure 4d shows the resonance shift of N_A as a function of reduced power exposure time. The resonance red shifts by 86 pm after exposure for 200 h, which corresponds to an increase of the GeSbS refractive index by 1.5×10^{-4}. The $1/e$ time constant of the exponential fit of the resonance shift is 89.5 h, consistent with the splitting relaxation. We further fit the resonance red shift to saturate after shifting 101 pm from the value obtained immediately after splitting, so that 81% of the initial shift remains.

While continuous reduced power exposure reduces both the splitting strength and the initial resonance wavelength shift by a maximum of ∼20%, these modifications remain modest. As shown in the Supporting Information, SI, not only does the rate of refractive index change depend on wavelength and optical intensity, but so does the maximum refractive index change, after which the photosensitivity saturates. At the reduced power levels used here, this saturation limits the drift of device characteristics.

RESONANCE SPLITTING ERASURE

The photosensitivity of chalcogenide glasses to visible light has been previously utilized to tune their refractive indices.[23,51] While the experiments in the previous sections consisted in using C-band infrared light injected into the device via GCs, here we use flood illumination with visible light at 561 nm, with a photon energy slightly below the 2.5 eV bandgap of the GeSbS glass.[52] As a consequence of the significantly increased absorption at this shorter wavelength, the high power levels obtained by means of waveguide confinement and resonant power enhancement are no longer required, so that flood illumination can be used. In this case the wavelength used to trigger the photosensitivity is no longer constrained by the resonance wavelengths of the ring.

The visible wavelength flood illumination is applied to device B after splitting S_B and after the short-term reliability test described earlier. As a consequence of the large refractive index changes induced by visible wavelength irradiation and the resulting progressive photosensitivity saturation, the resonant splitting can be erased. The previously unmodified refractive index regions are then preferentially written, reducing the index contrast.

We use a 561 nm wavelength fiber-coupled laser as the illumination source. Light is coupled into a standard single mode C-band fiber (which is multimode at 561 nm) of a fiber array located ∼20 μm over the surface of the chip and scanned in a meandered pattern over a 70 μm × 70 μm square surface covering the 15 μm radius ring resonator and its immediate vicinity (Figure 5). A total of 1.20 mW is delivered at the end of the fiber, corresponding to a peak intensity of about 0.022 mW/μm^2 at the chip surface. The scan has 14 steps in both the x- and y-directions, with a 5 μm step size sufficiently small to uniformly cover the entire area. After completion of a 3 min loop, the total delivered energy per surface is estimated as 44 μJ/μm^2, about 7 orders of magnitude lower than the energy levels required at 1550 nm. After each loop, the spectrum of the ring is remeasured with the help of two other fibers that are realigned to the GCs, during which the 561 nm flood-illumination is interrupted. Since the flood-illumination is restricted to the immediate vicinity of the ring, direct exposure of the GCs as well as of neighboring devices to visible light is avoided, so that GC insertion losses are kept constant throughout the measurements. A similar approach has been applied to trim hybrid chalcogenide-silicon waveguides.[53]

Figure 6a shows the normalized transmission spectra of the split resonance S_B during the erasing process. The wavelength of the resonance undergoes a significant blue shift under the

https://dx.doi.org/10.1021/acsphotonics.9b01593
ACS Photonics 2020, 7, 499−511

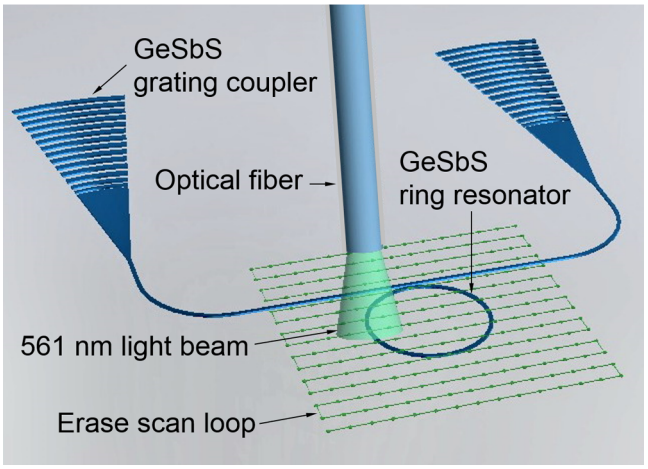

Figure 5. Schematic of the loop over which the fiber emitting 561 nm radiation is scanned for the flood-illumination process.

strong effect of visible light illumination. The splitting of S_B also disappears as the erasing process proceeds. Figure 6c shows the change of the splitting width and the corresponding Bragg grating reflectivity against erase loop number. The insets show exemplary spectra showing split resonances merging into one peak.

The overall resonance wavelength shift monitored via N_B and the corresponding refractive index change provide an insight on the grating erasure mechanism. It is apparent in Figure 6d that the extracted average GeSbS refractive index change slows down at higher loop numbers. For a sufficiently long exposure, the refractive index completely stops changing, as shown in Supporting Information, SI. This suggests that the structure may have found an intermediate bonding arrangement that no longer responds to the same light intensity. This shows that, for the large refractive index changes observed here, up to −0.02 after 35 erase cycles, the photosensitivity of the material eventually saturates. Furthermore, the dose response of photosensitivity becomes sublinear well before reaching saturation, which means that the regions of the grating that have already gone through a higher level of exposure have a lower photosensitivity than the remaining ones. Thus, flood exposure of the whole structure lessens the refractive index contrast of the material and eventually completely flattens its index profile. After 22 erase loops, the Bragg grating reflectivity becomes so small that the splitting is no longer resolved in the transmission spectra, even though the line width of the resonance continues to decrease as the two underlying lines merge. After 35 erase loops, the Bragg grating reflectivity reduces to 0.010, corresponding to 1.13×10^{-4} refractive index modulation.

The question may arise whether illumination-induced heating plays a role in the change of material properties seen here or whether this is due to direct photosensitivity. In the case of the previous experiments in which light was injected through the waveguide at C-band wavelengths, the emergence of a grating with small-scale periodicity rules out thermal effects as a primary cause. Moreover, the average refractive index change being on the same order as the index modulation strength points to the latter also being a consequence of direct photosensitivity. For the 561 nm wavelength flood illumination applied here, we made thermal simulations to estimate the

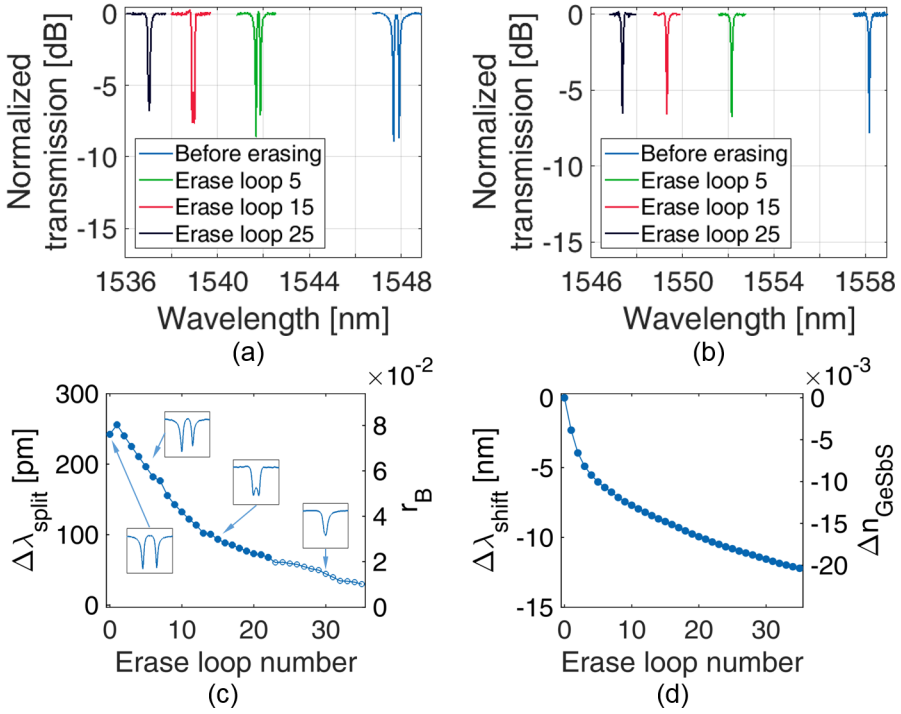

Figure 6. Resonance splitting erasure. Normalized transmission spectra of (a) the split resonance S_B and (b) the adjacent resonance N_B before and during flood illumination with 561 nm visible light. (c) Splitting width of S_B and corresponding Bragg grating field reflectivity against erase loop number. Solid dots are measured data. The hollow dots after 22 erase loops are obtained through resonance fitting, since splitting can no longer be directly read from the spectra once the resonances merge. Insets: enlargement of the normalized transmission spectra of resonance S_B in a wavelength range of 0.8 nm around the resonance and a normalized power range between −10 and 2 dB. (d) Wavelength shift of resonance N_B and corresponding GeSbS refractive index change against erase loop number.

https://dx.doi.org/10.1021/acsphotonics.9b01593
ACS Photonics 2020, 7, 499−511

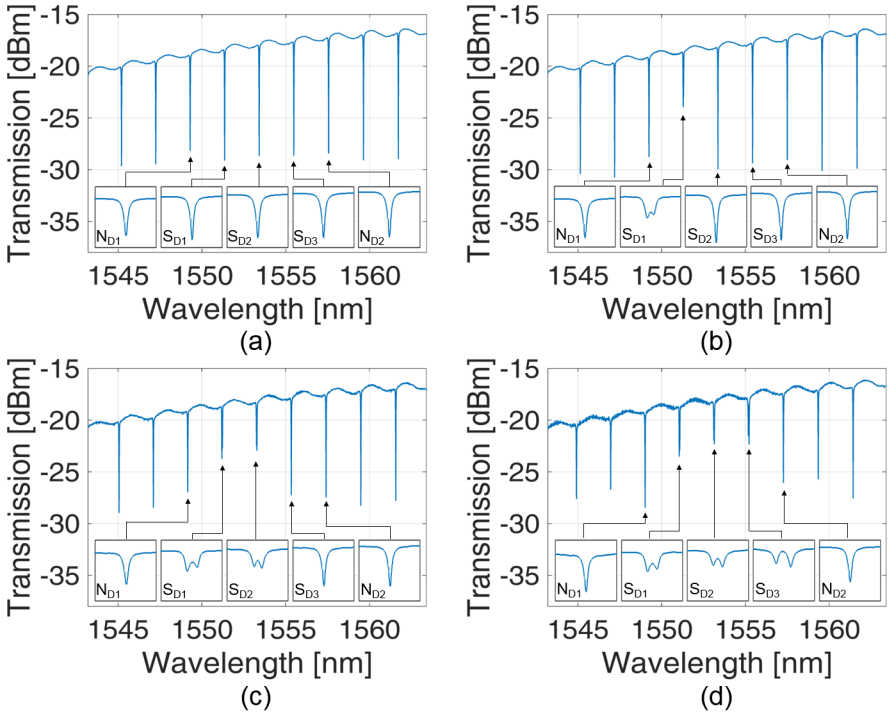

Figure 7. Transmission spectra of device D, before splitting (a) and after the splitting of resonances S_{D1} (b), S_{D2} (c), and S_{D3} (d). Insets: details of the transmission spectra of resonances N_{D1}, S_{D1}−S_{D3}, and N_{D2} in a 0.2 nm wavelength range and the power range −30 to −17 dBm.

Table 2. Measurement Results of the Splitting of Multiple Resonances[a]

				$\Delta\lambda_{split}$ (pm)			r_B		
splitting process	$\Delta\lambda_{shift}$ (pm)	Δn_{GeSbS}	Δn_B	S_{D1}	S_{D2}	S_{D3}	S_{D1}	S_{D2}	S_{D3}
1st splitting	−50	-0.8×10^{-4}	0.8×10^{-4}	23			0.036		
2nd splitting	−130	-2.2×10^{-4}	0.9×10^{-4}	32	27		0.049	0.042	
3rd splitting	−280	-4.7×10^{-4}	1.7×10^{-4}	32	30	50	0.049	0.048	0.077

[a] $\Delta\lambda_{shift}$: cumulative resonance wavelength shift; Δn_{GeSbS}: cumulative average GeSbS refractive index change; Δn_B: estimated refractive index contrast of the Bragg grating induced in the n^{th} splitting step; $\Delta\lambda_{split}$: splitting width; r_B: Bragg grating field reflectivity.

effect of heating. Assuming 10% of the light to be absorbed by the GeSbS waveguide, a very significant overestimate given that the assumed absorption coefficient of 3000 cm^{-1} is orders of magnitude higher than the reported coefficient at 561 nm,[33] we find that the temperature of the waveguide only rises by 10 °C. Given the thermo-optic coefficient reported in Supporting Information, SV, the resulting index change would still be 2 orders of magnitude below the measured one (Figure 6d). Thus, here too thermal effects can be safely ruled out from playing a dominant role over direct photosensitivity.

SELECTIVE MULTIPLE RESONANCE SPLITTING

Since in the range of refractive index changes relevant for resonance splitting, the photosensitivity is well below the saturation level (as shown in Supporting Information, SII), it is expected that several resonances can be split sequentially. Here we demonstrate sequential splitting of three resonances of device D.

Figure 7a shows the transmission spectrum before the splitting process. An FSR of 2.1 nm and a loaded Q-factor of 67000 lead to a power enhancement factor of 14.4 dB. The three resonances at the wavelengths 1551.3, 1553.4, and 1555.5 nm, labeled as S_{D1}, S_{D2}, and S_{D3}, are selected for the splitting demonstration. The resonances with the wavelengths 1549.2 and 1557.6 nm, which are immediately adjacent on either side of S_{D1}−S_{D3}, are labeled as N_{D1} and N_{D2} and are monitored to track the overall resonance wavelength shift as well as to verify the influence of the splitting processes on neighboring resonances. The 0.4 dB Fabry−Perot ripple in the transmission spectrum corresponds to 2.3% GC back-reflection. Table 2 summarizes results of the sequential splitting processes.

Following the resonance splitting process described above, we split S_{D1} by exposing it to light for 3 min with a power of 13.6 dBm inside the bus waveguide. The power intensity in the ring is estimated to be 116 MW/cm^2. The resulting splitting width is 23 pm (Figure 7b), which corresponds to a reflectivity of 0.036 and a Bragg grating refractive index modulation of 7.9×10^{-5}. Other resonances are not split.

Next, S_{D2} is split with light at its resonance wavelength dialed to a 13.8 dBm power in the bus waveguide, resulting in a similar intensity of 122 MW/cm^2 inside the ring, with a 4 min exposure time. Figure 7c displays the transmission spectrum after the second splitting. Both resonances S_{D1} and S_{D2} are split, which indicates that two superimposed Bragg gratings have been written in the ring. S_{D2} has a splitting width of 27 pm, which corresponds to the second Bragg grating's reflectivity to be 0.042 and to a refractive index modulation

https://dx.doi.org/10.1021/acsphotonics.9b01593
ACS Photonics 2020, 7, 499−511

of 9.3×10^{-5}. We can also observe that the splitting width of S_{D1} has increased from 23 to 32 pm.

Finally, S_{D3} is split with light at its resonance wavelength dialed to a 14.0 dBm power inside the bus waveguide. The power intensity inside the ring is estimated to be 128 MW/cm^2 and the splitting process is maintained for 7 min. All three resonances S_{D1}, S_{D2}, and S_{D3} are split (Figure 7d), showing that three superimposed Bragg gratings have been written. Resonance S_{D3} is split by 50 pm. The reflectivity and the refractive index modulation of the third Bragg grating are extracted to be 0.077 and 1.7×10^{-4}, respectively. The width of the splitting at resonance S_{D1} stays at the 32 pm seen after the second splitting process, while splitting of resonance S_{D2} increases from 27 to 30 pm.

The increase of the preapplied resonance splitting at each additional resonance splitting step may surprise at first. It has been pointed out that grating strengths might increase or decrease as successive gratings are being written depending on the convexity of the refractive index change versus exposure curve.[54] When the photosensitivity saturates, as seen here under very large refractive index changes, one would expect preexisting gratings to weaken rather than to strengthen as further gratings are being written. In our case, as shown in Supporting Information, SII, the induced refractive index change depends linearly on exposure time in the regime used here for Bragg grating inscription. The linearity of the refractive index change is further confirmed by the overall resonance frequency shifts as monitored with the resonances N_{D1} and N_{D2}: These blue shift by a cumulative amount of 50, 130, and 280 pm after the first, second, and third grating inscription step, with corresponding cumulative GeSbS refractive index changes of -0.8×10^{-4}, -2.2×10^{-4}, and -4.7×10^{-4} in line with the exposure times. Such a linear dose dependence enables gratings to be sequentially written without disrupting previously inscribed patterns.

Further insights are provided by the results reported by Arigiris et al.,[55] in which Bragg gratings were sequentially written in a photosensitive fiber. The study points out that the overlapping gratings lead to a slowly varying change of the refractive index modulation strength, so that some regions of the gratings are strengthened and others weakened. While this did not appear to change the maximum reflectivity at the Bragg wavelengths (as also predicted by eq 3, according to which the reduced grating length is compensated by an increased refractive index contrast), it was observed that the reflection band of the grating was widened, presumably as a consequence of the locally increased refractive index contrast in regions where multiple gratings were in phase (as also predicted by eq 2). This is a possible mechanism for the increase in splitting strength observed here compatible with the observed linear photosensitivity in our system.

Lastly, it may be observed that the estimated Δn_B are on the same order as the increments of the average refractive index changes ($[0.8,0.9,1.7] \times 10^{-4}$ vs $-[0.8,1.4,2.5] \times 10^{-4}$), confirming that a substantial amount of the average refractive index change is accounted for by the periodic components of the gratings. While in the ideal case of gratings with maximum contrast, one would have expected the peak-to-peak Δn_B to be twice the average refractive index shift, it should be noted that eq 3 is an approximation, as it estimates the reflectivity at the initial wavelength of the unsplit resonance (at the Bragg condition, with $\Delta\beta = 0$) and is thus overestimating the reflectivity at the split resonances, underestimating Δn_B. Combining eq 3 and eq 5 while linearizing tanh, one finds that the split resonances are close to the edges of the gratings' stopband (corresponding to $\Theta = 0$), showing that indeed the splitting is sufficiently large for the formulas to introduce some level of approximation.

DISCUSSION AND OUTLOOK

With a typical power enhancement factor of 12 dB inside the ring, grating inscription occurs with optical power levels on the order of 10 mW inside the bus waveguide, which are well in reach of what can be sourced by a semiconductor laser diode, even taking laser-to-chip coupling losses into account. Moreover, assuming the same power enhancement factor, induced gratings appear to be stable over extended periods of time for bus waveguide power levels on the order of 0.75 mW at resonance wavelengths. This power level is on the order of what is used in short distance fiber-optic data transmission and sufficiently high for data processing tasks. Advantageously, a laser spectrally aligned with the higher frequency resonance can be used to control the configuration of the device, while the lower frequency resonance can control the propagation of a probe beam, changing its attenuation, phase delay, or back-reflection. These would, for example, allow changing the weights in synaptic connections in an optical neural network,[20] or modifying the signal-combination network in a reservoir computing scheme.[21]

Directly using this device as a long-term reliable tunable back-reflector as part of an external cavity laser with high enough output power would probably require the device to be long-term stable under operation with much higher power levels, on the order of 10 or 20 mW, in order to be of practical relevance. To achieve this without increasing the power requirements for grating inscription, one could split the device into two vertically stacked rings, with a GeSbS ring fabricated on top of a planarized silicon nitride (SiN) photonic integrated circuit with a thin oxide cladding to allow evanescent coupling between the rings. Only a small portion of the power circulating in the SiN ring would reside in GeSbS, thereby enhancing the composite device's power handling capability. At the same time, direct injection of light into the GeSbS ring from a coupled GeSbS waveguide would still allow grating inscription at comparable power levels as reported here. While resonant frequencies of the two rings would be quite different, the GeSbS resonance with the targeted azimuthal number could be split, resulting in the targeted SiN resonator resonance with identical azimuthal number to also split. Since SiN resonators can have extremely high Q-factors,[56] evanescent probing of the grating is likely to split its resonances.

The erasure mechanism used here still has some limitations as it relies on driving the photosensitivity into partial saturation and thus cannot be repeatedly reapplied. Besides erasing the splitting via visible light flood illumination as done here, thermal annealing may be another potential way to erase the resonance splitting, since reversible photoinduced structural rearrangements triggered in chalcogenide glass can be removed by annealing to the glass-transition temperature.[57] This would overcome the present limitations, it remains however to be verified to what extent the photoinduced changes are fully reversible. Initial annealing of the films beyond the glass transition temperature could ensure that only reversible photoinduced changes are being later triggered. However, the magnitude of the thermally reversible photoinduced

https://dx.doi.org/10.1021/acsphotonics.9b01593
ACS Photonics 2020, 7, 499−511

changes might be significantly less than what was observed here, as we worked with as-deposited, nonannealed films that typically feature a larger amount of photosensitivity.[57] Moreover, repeated heating of the device to the glass transition temperature might cumulatively lead to a modification of its geometry, in which case encasing of the GeSbS material into a SiO_2 cladding, as done here for devices A, B, and D, would be advantageous.

CONCLUSIONS

We have demonstrated the splitting of multiple target resonances by inscribing superimposed Bragg gratings in GeSbS chalcogenide ring resonators with light at the target resonance frequencies at high power levels (>150 mW inside the ring). The stability of the resonance splitting in darkness and under reduced power operation (~10 mW inside the ring) was studied. While some degree of relaxation occurs in both cases, a large percentage of the initially induced splitting remains long-term stable. Furthermore, we managed to erase the resonance splitting using flood illumination with visible light at 561 nm and to subsequently reapply further resonance splitting.

We expect these devices to be of practical use in optical neural networks and reservoir computing schemes and, after some further adaptation, in silicon nitride based tunable reflectors for programmable external cavity lasers.

ASSOCIATED CONTENT

Supporting Information

The Supporting Information is available free of charge at https://pubs.acs.org/doi/10.1021/acsphotonics.9b01593.

Photosensitivity saturation under flood illumination with visible light, large resonance shift without saturation by injection of light at C-band resonance frequencies, back-reflection spectra of split resonances, resonance resplitting after erasure, thermally induced resonance shift, and long-term stability of split resonance in darkness and at room temperature (PDF)

AUTHOR INFORMATION

Corresponding Author

Jeremy Witzens − *Institute of Integrated Photonics, RWTH Aachen University, Aachen 52074, Germany;* orcid.org/0000-0002-2896-7243; Email: jwitzens@iph.rwth-aachen.de

Other Authors

Bin Shen − *Institute of Integrated Photonics, RWTH Aachen University, Aachen 52074, Germany*

Hongtao Lin − *College of Information Science & Electronic Engineering, Zhejiang University, Hangzhou, China*

Saeed Sharif Azadeh − *Institute of Integrated Photonics, RWTH Aachen University, Aachen 52074, Germany; Now at NINT Department, Max Planck Institute of Microstructure Physics, Halle 06120, Germany*

Jovana Nojic − *Institute of Integrated Photonics, RWTH Aachen University, Aachen 52074, Germany*

Myungkoo Kang − *College of Optics and Photonics, University of Central Florida, Orlando, Florida 32816-2700, United States;* orcid.org/0000-0003-4930-1683

Florian Merget − *Institute of Integrated Photonics, RWTH Aachen University, Aachen 52074, Germany*

Kathleen A. Richardson − *College of Optics and Photonics, University of Central Florida, Orlando, Florida 32816-2700, United States*

Juejun Hu − *Department of Materials Science and Engineering, Massachusetts Institute of Technology, Cambridge, Massachusetts 02139, United States*

Complete contact information is available at: https://pubs.acs.org/10.1021/acsphotonics.9b01593

Notes

The authors declare no competing financial interest.

REFERENCES

(1) Yi, X.; Xiao, Y.-F.; Feng, Y.; Qiu, D.-Y.; Fan, J.-Y.; Li, Y.; Gong, Q. Mode-splitting-based optical label-free biosensing with a biorecognition-covered microcavity. *J. Appl. Phys.* **2012**, *111*, 114702.

(2) Zhu, J.; Ozdemir, S. K.; Xiao, Y.-F.; Li, L.; He, L.; Chen, D.-R.; Yang, L. On-chip single nanoparticle detection and sizing by mode splitting in an ultrahigh-Q microresonator. *Nat. Photonics* **2010**, *4*, 46.

(3) Campanella, C. E.; Cuccovillo, A.; Campanella, C.; Yurt, A.; Passaro, V. M. N. Fibre Bragg Grating based strain sensors: review of technology and applications. *Sensors* **2018**, *18*, 3115.

(4) Kippenberg, T. J.; Spillane, S. M.; Vahala, K. J. Modal coupling in traveling-wave resonators. *Opt. Lett.* **2002**, *27*, 1669.

(5) Li, A.; Bogaerts, W. Backcoupling manipulation in silicon ring resonators. *Photonics Res.* **2018**, *6*, 620.

(6) Stern, B.; Ji, X.; Dutt, A.; Lipson, M. Compact narrow-linewidth integrated laser based on a low-loss silicon nitride ring resonator. *Opt. Lett.* **2017**, *42*, 4541−4544.

(7) Little, B. E.; Laine, J.-P.; Chu, S. T. Surface-roughness-induced contradirectional coupling in ring and disk resonators. *Opt. Lett.* **1997**, *22*, 4.

(8) Zhang, Z.; Dainese, M.; Wosinski, L.; Qiu, M. Resonance-splitting and enhanced notch depth in SOI ring resonators with mutual mode coupling. *Opt. Express* **2008**, *16*, 4621.

(9) Li, A.; van Vaerenbergh, T.; de Heyn, P.; Bienstman, P.; Bogaerts, W. Backscattering in silicon microring resonators: a quantitative analysis. *Laser Photon. Rev.* **2016**, *10*, 420−431.

(10) Zhu, J.; Ozdemir, S. K.; He, L.; Yang, L. Controlled manipulation of mode splitting in an optical microcavity by two Rayleigh scatterers. *Opt. Express* **2010**, *18*, 23535−23543.

(11) Chen, W.; Xiao, H.; Liu, Z.; Han, X.; Liao, M.; Zhao, T.; Tian, Y. Experimental realization of mode-splitting resonance using microring resonator with a feedback coupled waveguide. *Appl. Phys. Express* **2018**, *11*, 92201.

(12) Huang, Q.; Ma, K.; He, S. Experimental Demonstration of Single Mode-Splitting in Microring With Bragg Gratings. *IEEE Photonics Technol. Lett.* **2015**, *27*, 1402−1405.

(13) Shen, Y.; Divliansky, I. B.; Basov, D. N.; Mookherjea, S. Perfect set-and-forget alignment of silicon photonic resonators and interferometers. *Proc. Opt. Comm. Conf. (OFC), PDPC3*, OSA Publishing, 2011.

(14) Grillanda, S.; Raghunathan, V.; Singh, V.; Morichetti, F.; Michel, J.; Kimerling, L.; Melloni, A.; Agarwal, A. Post-fabrication trimming of athermal silicon waveguides. *Opt. Lett.* **2013**, *38*, 5450−5453.

(15) Spector, S.; Knecht, J. M.; Juodawlkis, P. W. Localized in situ cladding annealing for post-fabrication trimming of silicon photonic integrated circuits. *Opt. Express* **2016**, *24*, 5996−6003.

(16) Knights, A. P.; Wang, Z.; Paez, D.; Dow, L. Electrical trimming of the resonance of a silicon micro-ring resonator. *14th Int. Conf. on Group IV Photon., Germany* **2017**, 29−30.

(17) Romero-García, S.; Moscoso-Mártir, A.; Nojic, J.; Sharif-Azadeh, S.; Müller, J.; Shen, B.; Merget, F.; Witzens, J. Broadband, temperature tolerant and passively biased resonantly enhanced Mach-Zehnder modulators. *13th IEEE-NEMS, Singapore* **2018**, 1−7.

(18) Seok, T. J.; Quack, N.; Han, S.; Muller, R. S.; Wu, M. C. Large-scale broadband digital silicon photonic switches with vertical adiabatic couplers. *Optica* **2016**, *3*, 64.
(19) Rios, C.; Stegmaier, M.; Hosseini, P.; Wang, D.; Scherer, T.; Wright, C. D.; Bhaskaran, H.; Pernice, W. H. P. Integrated all-photonic non-volatile multi-level memory. *Nat. Photonics* **2015**, *9*, 725−732.
(20) Feldmann, J.; Youngblood, N.; Wright, C. D.; Bhaskaran, H.; Pernice, W. H. P. All-optical spiking neurosynaptic networks with self-learning capabilities. *Nature* **2019**, *569*, 208−214.
(21) Mesaritakis, C.; Papataxiarhis, V.; Syvridis, D. Micro ring resonators as building blocks for an all-optical high-speed reservoir-computing bit-pattern-recognition system. *J. Opt. Soc. Am. B* **2013**, *30*, 3048.
(22) Eggleton, B. J.; Luther-Davies, B.; Richardson, K. Chalcogenide photonics. *Nat. Photonics* **2011**, *5*, 141−148.
(23) Zoubir, A.; Richardson, M.; Rivero, C.; Schulte, A.; Lopez, C.; Richardson, K.; Hô, N.; Vallée, R. Direct femtosecond laser writing of waveguides in As_2S_3 thin films. *Opt. Lett.* **2004**, *29*, 748.
(24) Faraon, A.; Englund, D.; Bulla, D.; Luther-Davies, B.; Eggleton, B. J.; Stoltz, N.; Petroff, P.; Vučković, J. Local tuning of photonic crystal cavities using chalcogenide glasses. *Appl. Phys. Lett.* **2008**, *92*, 43123.
(25) Canciamilla, A.; Grillanda, S.; Morichetti, F.; Ferrari, C.; Hu, J.; Musgraves, J. D.; Richardson, K.; Agarwal, A.; Kimerling, L. C.; Melloni, A. Photo-induced trimming of coupled ring-resonator filters and delay lines in As_2S_3 chalcogenide glass. *Opt. Lett.* **2011**, *36*, 4002−4004.
(26) Hu, J.; Torregiani, M.; Morichetti, F.; Carlie, N.; Agarwal, A.; Richardson, K.; Kimerling, L. C.; Melloni, A. Resonant cavity-enhanced photosensitivity in As_2S_3 chalcogenide glass at 1550 nm telecommunication wavelength. *Opt. Lett.* **2010**, *35*, 874−876.
(27) Califa, R.; Munk, D.; Genish, H.; Kaganovskii, Y.; Bakish, I.; Rosenbluh, M.; Zadok, A. Large one-time photo-induced tuning of directional couplers in chalcogenide-on-silicon platform. *Opt. Express* **2015**, *23*, 28234−28243.
(28) Saliminia, A.; Villeneuve, A.; Galstyan, T. V.; LaRochelle, S.; Richardson, K. First- and second-order Bragg gratings in single-mode planar waveguides of chalcogenide glasses. *J. Lightwave Technol.* **1999**, *17*, 837−842.
(29) Baker, N. J.; Lee, H. W.; Littler, I. C.; de Sterke, C. M.; Eggleton, B. J.; Choi, D.-Y.; Madden, S.; Luther-Davies, B. Sampled Bragg gratings in chalcogenide (As_2S_3) rib-waveguides. *Opt. Express* **2006**, *14*, 9451.
(30) Ahmad, R.; Rochette, M. Photosensitivity at 1550 nm and Bragg grating inscription in As_2Se_3 chalcogenide microwires. *Appl. Phys. Lett.* **2011**, *99*, 61109.
(31) Zakery, A.; Elliott, S. R. Optical properties and applications of chalcogenide glasses: a review. *J. Non-Cryst. Solids* **2003**, *330*, 1−12.
(32) Musgraves, J. D.; Carlie, N.; Petit, L.; Boudebs, G.; Choi, J.; Richardson, M.; Richardson, K. Effect of Replacement of As by Ge and Sb on the Photo-Response under Near Infrared Femtosecond Laser Irradiation in As-based Sulfide Glasses. *Int. J. Appl. Glass Sci.* **2011**, *2*, 308−320.
(33) Anderson, T.; Petit, L.; Carlie, N.; Choi, J.; Hu, J.; Agarwal, A.; Kimerling, L.; Richardson, K.; Richardson, M. Femtosecond laser photo-response of $Ge_{23}Sb_7S_{70}$ films. *Opt. Express* **2008**, *16*, 20081−20098.
(34) Waldmann, M.; Musgraves, J. D.; Richardson, K.; Arnold, C. B. Structural properties of solution processed $Ge_{23}Sb_7S_{70}$ glass materials. *J. Mater. Chem.* **2012**, *22*, 17848.
(35) Singh, N.; Hudson, D. D.; Wang, R.; Mägi, E. C.; Choi, D.-Y.; Grillet, C.; Luther-Davies, B.; Madden, S.; Eggleton, B. J. Positive and negative phototunability of chalcogenide (AMTIR-1) microdisk resonator. *Opt. Express* **2015**, *23*, 8681−8686.
(36) Sohn, B.-U.; Kang, M.; Choi, J. W.; Agarwal, A. M.; Richardson, K.; Tan, D. T. H. Observation of very high order multi-photon absorption in GeSbS chalcogenide glass. *APL Photonics* **2019**, *4*, 36102.
(37) Serna, S.; Lin, H.; Alonso-Ramos, C.; Yadav, A.; Le Roux, X.; Richardson, K.; Cassan, E.; Dubreuil, N.; Hu, J.; Vivien, L. Nonlinear optical properties of integrated GeSbS chalcogenide waveguides. *Photonics Res.* **2018**, *6*, B37.
(38) Schwarz, C. M.; Grabill, C. N.; Richardson, G. D.; Labh, S.; Gleason, B.; Rivero-Baleine, C.; Richardson, K. A.; Pogrebnyakov, A.; Mayer, T. S.; Kuebler, S. M. Processing and fabrication of micro-structures by multiphoton lithography in germanium-doped arsenic selenide. *Opt. Mater. Express* **2018**, *8*, 1902.
(39) Shen, B.; Lin, H.; Merget, F.; Azadeh, S. S.; Li, C.; Lo, G.-Q.; Richardson, K. A.; Hu, J.; Witzens, J. Broadband couplers for hybrid silicon-chalcogenide glass photonic integrated circuits. *Opt. Express* **2019**, *27*, 13781.
(40) Hu, J.; Tarasov, V.; Agarwal, A.; Kimerling, L.; Carlie, N.; Petit, L.; Richardson, K. Fabrication and testing of planar chalcogenide waveguide integrated microfluidic sensor. *Opt. Express* **2007**, *15*, 2307−2314.
(41) Du, Q.; Huang, Y.; Li, J.; Kita, D.; Michon, J.; Lin, H.; Li, L.; Novak, S.; Richardson, K.; Zhang, W.; et al. Low-loss photonic device in Ge-Sb-S chalcogenide glass. *Opt. Lett.* **2016**, *41*, 3090−3093.
(42) Brovelli, L. R.; Keller, U. Simple analytical expressions for the reflectivity and the penetration depth of a Bragg mirror between arbitrary media. *Opt. Commun.* **1995**, *116*, 343−350.
(43) Skaar, J. Fiber Bragg Gratings: Analysis and Synthesis Techniques. *Fiber Bragg Grating Sensors: Recent Advancements, Industrial Applications and Market Exploitation*; Bentham Science Publishers Ltd: Sharja, U.A.E., 2015.
(44) Robinson, J. T.; Preston, K.; Painter, O.; Lipson, M. First-principle derivation of gain in high-index-contrast waveguides. *Opt. Express* **2008**, *16*, 16659−16669.
(45) Witzens, J. High-Speed Silicon Photonics Modulators. *Proc. IEEE* **2018**, *106*, 2158−2182.
(46) Geiger, S.; Du, Q.; Huang, B.; Shalaginov, M. Y.; Michon, J.; Lin, H.; Gu, T.; Yadav, A.; Richardson, K. A.; Jia, X.; et al. Understanding aging in chalcogenide glass thin films using precision resonant cavity refractometry. *Opt. Mater. Express* **2019**, *9*, 2252.
(47) Li, Q.; Zhang, Z.; Wang, J.; Qiu, M.; Su, Y. Fast light in silicon ring resonator with resonance-splitting. *Opt. Express* **2009**, *17*, 933.
(48) Little, B. E.; Chu, S. T.; Haus, H. A.; Foresi, J.; Laine, J.-P. Microring resonator channel dropping filters. *J. Lightwave Technol.* **1997**, *15*, 998−1005.
(49) Gleason, B.; Richardson, K.; Sisken, L.; Smith, C. Refractive Index and Thermo-Optic Coefficients of Ge-As-Se Chalcogenide Glasses. *Int. J. Appl. Glass Sci.* **2016**, *7*, 374−383.
(50) Krecmer, P.; Moulin, A. M.; Stephenson, R. J.; Rayment, T.; Welland, M. E.; Elliott, S. R. Reversible Nanocontraction and Dilatation in a Solid Induced by Polarized Light. *Science* **1997**, *277*, 1799−1802.
(51) Lee, M. W.; Grillet, C.; Smith, C. L. C.; Moss, D. J.; Eggleton, B. J.; Freeman, D.; Luther-Davies, B.; Madden, S.; Rode, A.; Ruan, Y.; et al. Photosensitive post tuning of chalcogenide photonic crystal waveguides. *Opt. Express* **2007**, *15*, 1277.
(52) Choi, J. W.; Han, Z.; Sohn, B.-U.; Chen, G. F. R.; Smith, C.; Kimerling, L. C.; Richardson, K. A.; Agarwal, A. M.; Tan, D. T. H. Nonlinear characterization of GeSbS chalcogenide glass waveguides. *Sci. Rep.* **2016**, *6*, 39234.
(53) Canciamilla, A.; Morichetti, F.; Grillanda, S.; Velha, P.; Sorel, M.; Singh, V.; Agarwal, A.; Kimerling, L. C.; Melloni, A. Photo-induced trimming of chalcogenide-assisted silicon waveguides. *Opt. Express* **2012**, *20*, 15807−15817.
(54) Meghavoryan, D. M.; Daryan, A. V. Superimposed fiber Bragg grating simulation by the method of single expression for optical CDMA systems. *IEEE Photonics Technol. Lett.* **2003**, *15*, 1546−1548.
(55) Arigiris, A.; Konstantaki, M.; Ikiades, A.; Chronis, D.; Florias, P.; Kallimani, K.; Pagiatakis, G. Fabrication of high-reflectivity superimposed multiple-fiber Bragg gratings with unequal wavelength spacing. *Opt. Lett.* **2002**, *27*, 1306.
(56) Pfeiffer, M. H. P.; Kordts, A.; Brasch, V.; Zervas, M.; Geiselmann, M.; Jost, J. D.; Kippenberg, T. Photonic Damascene

process for integrated high-Q microresonator based nonlinear photonics. *Optica* **2016**, *3*, 20−25.
(57) Elliott, S. R. A unified model for reversible photostructural effects in chalcogenide glasses. *J. Non-Cryst. Solids* **1986**, *81*, 71−98.

https://dx.doi.org/10.1021/acsphotonics.9b01593
ACS Photonics 2020, 7, 499−511